Constraining the AGN Contribution in a Multiwavelength Study of Seyfert Galaxies

M. Meléndez, S.B. Kraemer

Institute for Astrophysics and Computational Sciences, Department of Physics, The Catholic University of America, Washington, DC

07melendez@cua.edu

H.R. Schmitt

Remote Sensing Division, Naval Research Laboratory, Washington, DC

and

Interferometrics, Inc., Herndon, VA

D.M. Crenshaw

Department of Physics and Astronomy, Georgia State University, Atlanta, GA

R.P. Deo

Department of Physics, Drexel University, Philadelphia, PA

R.F. Mushotzky

NASA/Goddard Space Flight Center, Greenbelt , MD

and

F.C. Bruhweiler

Institute for Astrophysics and Computational Sciences, Department of Physics, The Catholic University of America, Washington, DC

ABSTRACT

We have studied the relationship between the high- and low-ionization [O IV] λ25.89 μm, [Ne III] λ15.56 μm and [Ne II] λ12.81 μm emission lines with the aim of constraining the active galactic nuclei (AGN) and star formation contributions for a sample of 103 Seyfert galaxies. We used the [O IV] and [Ne II]

emission as tracers for the AGN power and star formation to investigate the ionization state of the emission-line gas. We find that Seyfert 2 galaxies have, on average, lower [O IV]/[Ne II] ratios than those of Seyfert 1 galaxies. This result suggests two possible scenarios: 1) Seyfert 2 galaxies have intrinsically weaker AGN, or 2) Seyfert 2 galaxies have relatively higher star formation rates than Seyfert 1 galaxies. We estimate the fraction of [Ne II] directly associated with the AGN and find that Seyfert 2 galaxies have a larger contribution from star formation, by a factor of $\sim$ 1.5 on average, than what is found in Seyfert 1 galaxies. Using the stellar component of [Ne II] as a tracer of the current star formation we found similar star formation rates in Seyfert 1 and Seyfert 2 galaxies. We examined the mid- and far-infrared continua and find that [Ne II] is well correlated with the continuum luminosity at 60μm and that both [Ne III] and [O IV] are better correlated with the 25μm luminosities than with the continuum at longer wavelengths, suggesting that the mid-infrared continuum luminosity is dominated by the AGN, while the far-infrared luminosity is dominated by star formation. Overall, these results test the unified model of AGN, and suggest that the differences between Seyfert galaxies cannot be solely due to viewing angle dependence.

Subject headings: Galaxy: stellar content — galaxies: Seyfert — infrared: galaxies

1. Introduction

Active Galactic Nuclei (AGN) are thought to harbor massive black holes surrounded by an accretion disk responsible for the enormous energy rates observed in their unresolved nuclei (Rees 1984; Peterson & Wandel 2000; Peterson et al. 2004). Historically, Seyfert 1 and Seyfert 2 galaxies have been classified by the presence or absence of broad optical emission lines. In this regard, Seyfert 1 galaxies have broad permitted (FWHM$\sim$ 1-5$\times10^3$ km s^{-1}) and narrow (FWHM$\sim$ 5$\times10^2$ km s^{-1}) permitted and forbidden lines and Seyfert 2 galaxies have only narrow permitted and forbidden line emission (Khachikian & Weedman 1974). Using spectropolarimetry, Antonucci & Miller (1985) found broad Balmer lines and [Fe II] emission in the polarized spectrum of the Seyfert 2 NGC 1068 galaxy, characteristic of a Seyfert 1 spectrum. This represents the first observational evidence in favor of a unified model. In this model, Seyfert 1 and Seyfert 2 galaxies are intrinsically the same with their differences attributed to viewing angle. In Seyfert 2 galaxies, our line of sight to the broad line region (BLR) and the central engine is obstructed by an optically thick dusty torus-like

structure, while in Seyfert 1 galaxies, our line of sight is not obstructed by the torus, allowing a direct view of the central regions of the active galaxy.

Although it has been observationally confirmed, the unified model for Seyfert galaxies does not address the role of stellar activity. The fact that active galaxies can also host massive star-forming regions (e.g, Terlevich et al. 1990; Maiolino et al. 1997, 1998; Cid Fernandes et al. 2004; Gu et al. 2006; Davies et al. 2007) suggests a connection between the AGN and star formation in the proximity of the super-massive black hole, typically on scales of a few hundred parsecs. These starbursts may have a significant impact on the fueling of the central black hole (e.g., Schmitt et al. 1999; Davies et al. 2007). Many authors have suggested that violent star formation, in the circumnuclear region, plays a fundamental role in the energetics of Seyfert 2 galaxies (e.g., Terlevich & Melnick 1985; Maiolino et al. 1998; Cid Fernandes & Terlevich 1995; González Delgado et al. 2001; Cid Fernandes et al. 2001). This extra source of energy, a young stellar population in the vicinity of the nucleus, could complement the non-stellar component associated with the AGN. Maiolino et al. (1997) suggested that asymmetric morphologies and bars, especially in Seyfert 2 galaxies, are an important factor in star formation and Seyfert classification. These asymmetric morphologies can induce radial gas inflow and fueling of the nuclear region, thus obscuring and feeding the active nucleus. González Delgado et al. (2001) discuss the possibility of two kinds of Seyfert 2 galaxies based on their stellar population properties: those with young and intermediate age stars and those with the optical continuum dominated by old stars.

In principle, the richness of the infrared spectrum provides a unique opportunity to test the unified model of AGN, since the mid- and far-infrared spectra appear to be different in Seyfert 1 and Seyfert 2 galaxies (e.g., Sanders et al. 1988; Pier & Krolik 1992; Antonucci 1993; Clavel et al. 2000; Armus et al. 2007). However, there is the technical difficulty of isolating the AGN from contamination by the host galaxy emission and, more importantly, star formation features (e.g., Lutz et al. 2004; Weedman et al. 2005). In this work we will focus on deconvolving the different contributions (e.g., AGN+star formation) in the [Ne II] λ12.81 μm emission line and the mid- and far-infrared continua. In order to estimate the component associated with the AGN we will use the high-ionization potential ($\sim$ 54.9 eV) [O IV] λ25.89 μm emission line. We found (Meléndez et al. 2008, hereafter M08) a tight correlation in Seyfert 1 galaxies between the [O IV] and the X-ray 14-195 keV continuum luminosities from *Swift*/BAT observations (Markwardt et al. 2005). A weaker correlation was found in Seyfert 2 galaxies, which was due to partial absorption in the 14-195 keV band. Overall, we proposed [O IV] as a truly isotropic property of AGNs given its high ionization potential and that is basically unaffected by reddening, meaning that the [O IV] strength directly measures the AGN power. In this work we will isolate the stellar component of the [Ne II] emission to trace the instantaneous star formation rates in our

sample of Seyfert galaxies.

2. The Infrared Sample

Our sample of Seyfert galaxies includes compilations from Deo et al. (2007), Tommasin et al. (2008), Sturm et al. (2002), Weedman et al. (2005) and the X-ray selected sample from M08. This sample has been expanded to include [O IV] λ25.89 μm, [Ne II] λ12.81 μm and [Ne III] λ15.56 μm fluxes from our analysis of unpublished archival spectra observed with the Infrared Spectrograph (IRS) (see Houck et al. 2004) on board *Spitzer* in the 1st Long-Low (LL1, λ = 19.5 - 38.0 μm, 10.7$''$ $\times$ 168$''$, $R \sim 60 - 127$), Short-High (SH, λ = 9.9 - 19.6 μm, 4.7$''$ $\times$ 11.3$''$,$R \sim 600$) and Long-High (LH, λ = 18.7 - 37.2 μm, 11.1$''$ $\times$ 22.3$''$, $R \sim 600$) IRS order in Staring mode. The sample includes 64 Seyfert 2 and 39 Seyfert 1 galaxies which are listed in Table 1. The infrared luminosities are presented without reddening corrections. For comparison, we searched the literature for the Seyfert 1 and Seyfert 2 galaxies with measured mid- and far-infrared continuum fluxes at 25μm, 60μm and 100μm from the *Infrared Astronomical Satellite* (*IRAS*) (Neugebauer et al. 1984; Soifer et al. 1989; Moshir et al. 1990; Sanders et al. 2003). Note that it was not possible to find *IRAS* fluxes for all galaxies in the sample. For the analysis of the mid-infrared emission lines observed with IRS/*Spitzer* we followed the procedure described in M08.

First, we need to confirm that our sample, which was compiled from various sources, was not biased in terms of luminosity, e.g., toward high luminosity Seyfert 1 and/or low-luminosity Seyfert 2 galaxies. This test was made by comparing the different luminosities for both the mid-infrared emission lines and continuum luminosities for the two groups of galaxies. The results from these comparisons are shown in Figure 1 with the results from the Kolmogorov-Smirnov (K-S) test presented in Table 2. This table also includes information about the numbers of Seyfert 1 and Seyfert 2 galaxies, mean values and standard deviations of the mean for the measured quantities.

The histograms of [Ne II], [Ne III] and [O IV] luminosities are presented in Figure 1. From the [Ne II] histogram it can be seen that Seyfert 1 and Seyfert 2 galaxies have similar distributions of values. The K-S test for this emission line luminosity returns a $\sim$ 79.0% probability of the null hypothesis (i.e., that there is no difference between Seyfert 1 and Seyfert 2 galaxies), or in other words, two samples drawn from the same parent population would differ this much $\sim$ 79.0% of the time[1]. From the distribution of [Ne III] luminosities

[1]A probability value of less than 5% represents a high level of significance that two samples drawn from the same population are different. A strong level of significance is obtained for values smaller than 1% (e.g.,

one can see the relative absence of low luminosity Seyfert 1 as compared with Seyfert 2 galaxies. For $L_{[\mathrm{Ne\ III}]} < 40.5$ there are 20 Seyfert 2 galaxies (comprising $\sim 30\%$ of the Seyfert 2 sample) and only four Seyfert 1 galaxies ($\sim 10\%$ of the Seyfert 1 sample). This may suggest the presence of intrinsically weaker AGN in the Seyfert 2 galaxies. However, the K-S result returns $\sim 22.8\%$ probability of the null hypothesis, indicating that the apparent differences between the two groups are not statistically significant. From the [O IV] histogram one can seen a lack of low luminosity Seyfert 1 ($L_{[\mathrm{O\ IV}]} < 40.5$) as compared with Seyfert 2 galaxies, similar to that found in the distribution of [Ne III] luminosities, with 20 Seyfert 2 galaxies comprising $\sim 30\%$ of the Seyfert 2 sample and only five Seyfert 1 galaxies ($\sim 13\%$ of the Seyfert 1 sample). However, the K-S result returns a $\sim 10.0\%$ probability of the null hypothesis. Overall, we found that the mid-infrared luminosity distributions for Seyfert 1 and Seyfert 2 galaxies are statistically similar, even with the absence of low luminosity Seyfert 1 galaxies in the [Ne III] and [O IV] distributions.

We also studied the infrared emission continuum properties of the sample using the 25μm, 60μm, 100μm and far-infrared (FIR) luminosities. It should be noted that the large beam infrared spectral energy distributions from *IRAS* (with a field of view of $0.75' \times 4.6'$ at 25μm, $1.5' \times 4.7'$ at 60μm and $3.0' \times 5.0'$ at 100μm) includes the AGN continuum and the host galaxy emission (Spinoglio et al. 1995; Lutz et al. 2004). The far-infrared luminosity (FIR) is characterized by the emission at 60 μm and 100 μm (e.g., Condon 1992; Sanders & Mirabel 1996). In this regard, the 60 μm emission represents a "warm" component associated with dust around young star-forming regions. On the other hand, cooler "cirrus" emission at 100 μm (Low et al. 1984) is associated with a more extended dust heated by the interstellar radiation field (Kennicutt 1998).

The histograms of 25 μm ($L_{25\mu\mathrm{m}}$), 60 μm ($L_{60\mu\mathrm{m}}$) and far-infrared, FIR μm (L_{FIR}), continuum luminosities are presented in Figure 2. Overall, it can be seen that Seyfert 1 and Seyfert 2 galaxies have a similar distribution of values. For the 25 μm luminosities distributions the K-S test returns a $\sim 27.3\%$ probability of the null hypothesis. For the 60 μm luminosity ($L_{60\mu\mathrm{m}}$) the K-S test returns $\sim 70.4\%$ probability of the null hypothesis. This result is in agreement with previous studies that have assumed that the 60 μm continuum emission is an isotropic quantity (e.g., Schmitt et al. 2001). However, this assumption must be adopted with caution because the torus emission may be anisotropic at 60 μm (Pier & Krolik 1992). Figure 2 shows that Seyfert 1 and Seyfert 2 galaxies also have similar distributions in the FIR. The K-S test returns a $\sim 51.3\%$ probability of the null hypothesis for the FIR distribution.

Press et al. 1992; Bevington & Robinson 2003)

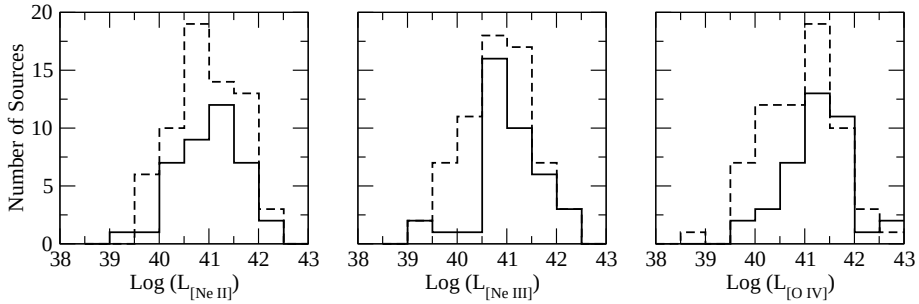

Fig. 1.— Comparison of the [Ne II], [Ne III] and [O IV] luminosities in Seyfert 1 (*solid line*) and Seyfert 2 (*dashed line*) galaxies. This sample includes 39 Seyfert 1 and 65 Seyfert 2 galaxies. The K-S test for these emission line luminosities show that two samples drawn from the same population would differ this much $\sim$ 79.0%, $\sim$ 22.8% and $\sim$ 10.0% of the time for the [Ne II], [Ne III] and [O IV] luminosity distributions, respectively.

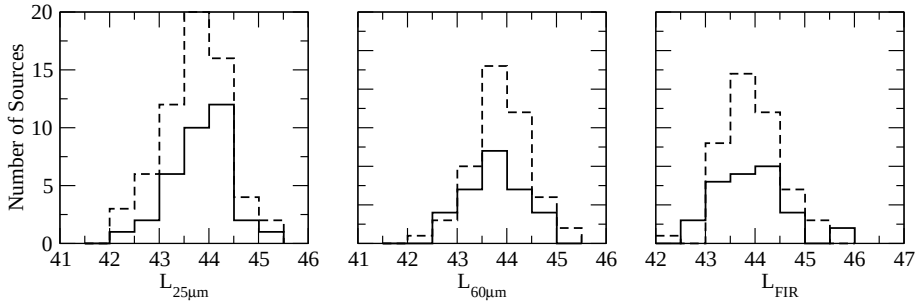

Fig. 2.— Comparison of the 25μm, 60μm and FIR luminosities in Seyfert 1 (*solid line*) and Seyfert 2 (*dashed line*) galaxies. This sample includes 36 Seyfert 1 and 63 Seyfert 2 galaxies. The K-S test for these continuum luminosities returns $\sim$ 27.3%, $\sim$ 70.4% and $\sim$ 51.3% probability of the null hypothesis for the 25μm, 60μm and FIR continuum luminosities distributions, respectively.

In spite of the fact that Seyfert 1 and Seyfert 2 galaxies have similar distributions of infrared luminosities, using the observed mid- and far-infrared continuum fluxes, we found a clear difference in their spectral index[2] α_{25-60} in Seyfert 1 and Seyfert 2 galaxies, as shown in Figure 3. The K-S test returns $\sim 0.1\%$ probability of the null hypothesis. The spectral shape between 25μm and 60μm has been used to separate Ultraluminous Infrared Galaxies (ULIRGs) that are "warm" and possibly dominated by the AGN and those that are "cold" and likely to be dominated by star formation (Sanders et al. 1988; Armus et al. 2007). From our sample, we found that Seyfert 2 galaxies possess relatively cooler dust, with an average $\alpha_{25-60} = -1.5 \pm 0.1$, than Seyfert 1 galaxies, $\alpha_{25-60} = -0.8 \pm 0.1$, in agreement with previous findings by Ho et al. (2003). This result suggests that the infrared spectra of Seyfert 1 galaxies are dominated by hot dust heated by the AGN (e.g., Heisler et al. 1997; González Delgado et al. 2001).

3. Emission Line Diagnostics

The ratios of high- and low-ionization mid-infrared emission lines have been widely used to separate the relative contribution of the AGN and star formation (e.g., Genzel et al. 1998; Sturm et al. 2002; Dale et al. 2006). We performed a statistical analysis for the [O IV]/[Ne II], [Ne III]/[Ne II] and [O IV]/[Ne III] ratios for our sample of 103 Seyfert galaxies, with the results presented in Table 2. Figure 4 shows the histograms of [O IV]/[Ne II], [O IV]/[Ne III] and [Ne III]/[Ne II] ratios. From the [O IV]/[Ne II] ratios, it can be seen that Seyfert 2 galaxies are displaced toward smaller values than those found for Seyfert 1's, in agreement with previous findings by Deo et al. (2007). Accordingly, in the sample, Seyfert 2 galaxies have, on average, smaller [O IV]/[Ne II] ratios than those observed in Seyfert 1 galaxies. The K-S test returns $\sim 0.9\%$ probability of the null hypothesis, indicating, that the two Seyfert groups are statistically different. As for [Ne III]/[Ne II], Seyfert 2 galaxies are again displaced toward values smaller than those found for Seyfert 1 galaxies, with the majority of Seyfert 2 galaxies ($\sim 60\%$ of the Seyfert 2 population) having [Ne III]/[Ne II] < 1.0. The K-S test returns $\sim 1.1\%$ probability of the null hypothesis. From the histogram of [O IV]/[Ne III], it can be seen that both groups of galaxies have similar distributions. The K-S test returns a $\sim 37.7\%$ probability of the null hypothesis. This result suggests that [Ne III] is also an isotropic quantity and could be used to estimate AGN power (e.g., Deo et al. 2007; Gorjian et al. 2007; Tommasin et al. 2008).

In Figure 5 we compare the [O IV]/[Ne II] and [Ne III]/[Ne II] ratios in Seyfert 1

[2]The continuum is assumed to be a power law, $F_\nu \propto \nu^\alpha$, where α is the spectral index

and Seyfert 2 galaxies, where the Spearman rank test returned a strong correlation ($r_s = 0.810$ $P_r = 1.0 \times 10^{-15}$). This strong correlation supports the utility of the [Ne III]/[Ne II] ratio as a diagnostic of the relative strength of the AGN as found by Tommasin et al. (2008). From this correlation we found that Seyfert 2 galaxies show lower [O IV]/[Ne II] and [Ne III]/[Ne II] ratios than Seyfert 1 galaxies. As suggested by Deo et al. (2007), one needs to consider two possible scenarios. 1) Seyfert 1 galaxies have more highly ionized narrow line regions (NLR) than Seyfert 2 galaxies resulting in an apparently weaker AGN in Seyfert 2 galaxies; 2) Seyfert 2 galaxies have a relatively higher star formation rates than Seyfert 1 galaxies normalized to the AGN luminosity. In the former scenario, one needs to consider that there could be a source of obscuration on a much larger scale that is affecting the [O IV] but not the [Ne II] emission; however, this possibility contradicts the findings of [O IV] as a true isotropic quantity for the AGN (see M08). Alternatively, this hidden inner NLR scenario is ruled out by Deo et al. (2007) where they found the amount of extinction in the mid-infrared for Seyfert 1.8/1.9s to be negligible.

We found that Seyfert 1 and Seyfert 2 galaxies are statistically different in their relative contribution of the AGN and star formation, as given by the analysis of their [O IV]/[Ne II] and [Ne III]/[Ne II] ratios. Nevertheless, one needs to check if the emission-line ratios are not biased because of the relative absence of low luminosity Seyfert 1 galaxies in our sample. In this regard, the poor correlation found ($r_s = 0.489$ $P_r = 9.7 \times 10^{-7}$) between [O IV]/[Ne II] and [O IV] luminosities, and the fact that the K-S test results for the [O IV] and [Ne III] luminosity distribution indicated that both groups have statistically similar distributions (see discussion in Section 2), indicates that our emission-line ratios are not biased because of the relative absence of low luminosity Seyfert 1 galaxies in our sample. The [O IV]/[Ne II] emission line ratio was also compared with the redshift (z) in order to check if our previous results are biased towards small ratios at higher values of z, given the fact that [O IV] is likely to be produced in a compact region, whereas [Ne II] could be produced in a more extended region. The Spearman rank r_s test did not show any correlation ($r_s = -0.075$, $P_r = 0.68$) with z. At the median redshift for the sample, $z = 0.02$, $1''$ represents ∼400 pc for $H_o = 71$ km s^{-1} Mpc^{-1}. Hence, for example, the SH slit will sample about ∼2 kpc in the dispersion direction at z of 0.02.

4. Deconvolving the Stellar Contribution to the [Ne II] emission

In Figure 6 we compare [Ne II] and [O IV] fluxes and luminosities. There appear to be a relative deficiency of Seyfert 1 galaxies in the upper left region of the plot. In the plot we identified some of the outliers in the sample. All these sources show strong

star formation activity, and have also been classified as starburst galaxies or to harbor massive H II regions. These galaxies show strong polycyclic aromatic hydrocarbon (PAH) features at 6.2 μm and 11.5 μm (Deo et al. 2007; Tommasin et al. 2008). PAHs are a class of large organic molecules that have been observationally associated with star formation (e.g., Clavel et al. 2000; Förster Schreiber et al. 2004; Calzetti et al. 2005; Schweitzer et al. 2006). The strong [Ne II] in these objects indicates that [Ne II] is a quantitative tracer of star formation. Results from the statistical analysis are presented in Table 3. One should note that, due to redshift effects, luminosity-luminosity plots will almost always show some correlation. Thus, we are primarily interested in the tightness of the correlations or the slopes (e.g., of one class versus another).

Figure 7 shows the correlation between the [O IV] and [Ne III] in fluxes (left) and luminosities (right), where a tight and strong correlation is seen (also, see Table 3). This result corroborates the effectiveness of [Ne III] as a tracer of the AGN power as discussed by Gorjian et al. (2007), who found a strong correlation between [Ne V]λ14.3 μm emission-line, which originates from an ion with an ionization potential of $\sim$ 97 eV and thus is due almost entirely to AGN photoionization (Abel & Satyapal 2008), and [Ne III]. Although, there is evidence of [Ne III] emission from stars (e.g., Ho & Keto 2007), the tight correlation between the [O IV] and [Ne III] suggest that this contribution is minimal in our AGN sample. In this regard, Figure 7 also shows 11 "pure" AGN sources (see Table 1), i.e., sources that shows no detectable PAH features at 6.2 μm and 11.5 μm in their spectra. One can see the similarity between the full sample and the pure AGN linear fits. The linear regression values for the pure AGN sources are given in Table 4.

Assuming that the observed [Ne II] emission is composed of both an AGN and a stellar component, we estimated the star formation contribution (SC) in the [Ne II] emission by subtracting the predicted [Ne II] that is produced by the AGN. In this regard, the predicted [Ne II] emission associated with the AGN was obtained from the linear regression for the pure AGN sources from the observed [Ne II] - [O IV] correlation in luminosities.

Figure 8 shows the correlation between [Ne II] and [O IV] luminosities. The different dashed lines represent the percentage of star formation contribution in the observed [Ne II] emission lines. Table 1 shows the percentage of star formation contribution, SC (%), in the [Ne II] observed luminosity. For example, NGC 7469 and NGC 3079 are known to harbor regions of enhanced star formation (Perez-Olea & Colina 1996; Genzel et al. 1998; Weedman et al. 2005). In these galaxies, the AGN contributes $\sim$ 12% for NGC 7469 and $\sim$ 18% for NGC 3079 to the observed [Ne II] flux. These results are in agreement with the strong PAH 6.2 μm ($F_{6.2\mu\mathrm{m}} > 5.3 \times 10^{-19}$W cm^{-2}) observed in these objects by Deo et al. (2007). Genzel et al. (1998) generated an empirical diagram (mixing model) to separate the

AGN from galaxies powered by enhanced star formation, by using the ratio of high- and low-ionization mid-infrared lines and PAH features. We compared their results with values obtained in the present work for our sample. For example, Genzel et al. (1998) find that Mrk 273 has an AGN contribution of $\sim$ 40%, compared with $\sim$ 34% from our empirical diagnostic. The Seyfert galaxies NGC 4151, NGC 1068, NGC 5506 and NGC 3783 are AGN dominated, i.e., more than 75% of the [Ne II]'s contribution from the AGN, as suggested by previous mixing models (Genzel et al. 1998; Sturm et al. 2002). These results are in excellent agreement with the star formation and AGN contribution values that we obtained from these objects (see Table 1). The Seyfert 2 galaxy, NGC 6240, is dominated by star formation (Lutz et al. 1996; Genzel et al. 1998) in agreement with our value of a $\sim$ 90% stellar contribution to the [Ne II] emission line. We estimated an error of $\sim$ 20% in the AGN-predicted [Ne II] luminosities, based on the star formation contribution obtained for Mrk 3, which is one of the objects with no detectable PAH at 6.2μm (Deo et al. 2007).

Table 2 shows the results from the statistical analysis for the star formation contribution in the [Ne II] emission. We found that, averaged over populations, Seyfert 2 galaxies have a stronger stellar contribution in their [Ne II] observed emission line, $\sim 43 \pm 4\%$, than that found in Seyfert 1 galaxies, $\sim 28 \pm 5\%$. The K-S test returns $\sim$ 4.4% probability of the null hypothesis, meaning that the two groups of Seyfert galaxies are statistically different in their relative stellar contribution to their [Ne II] emission, despite the fact that there are Seyfert 1 galaxies in our sample with strong starbursts (e.g., NGC 7469). Nevertheless, these results are in agreement with previous findings where Seyfert 2 galaxies typically show stronger starburst signatures in their infrared spectra than Seyfert 1 galaxies (e.g., Buchanan et al. 2006).

In Figure 9 we plot the result from the deconvolution method performed to the observed [Ne II] emission. In the upper, middle and lower panel we present the observed (AGN+stellar component), the AGN-only, and the stellar component for [Ne II] versus [Ne III] emission line luminosities. In order to avoid a misleadingly linear correlation, we plotted the observed, stellar and AGN components of [Ne II] against [Ne III]. A tight correlation between [Ne III] and the pure AGN [Ne II] validates the method used to untangle the different contributions in the [Ne II] emission line. In the lower panels of these plots, one note the lack of correlation between the stellar component of [Ne II] and the strength of the AGN, as characterized by the [Ne III] emission.

5. Star Formation Rate

Using a sample of non-AGN star-forming galaxies, Ho & Keto (2007) investigated the utility of the mid-infrared emission lines of [Ne II] and [Ne III] as a star formation rate (SFR) indicator, given the fact that the Lyman continuum radiation, which can ionize Ne^{+} and Ne^{2+}, is mainly produced by young stars. In order to calculate the SFR we have used the stellar component of [Ne II], as deconvolved from the previous analysis, and assumed $f_{+} = 0.75$ and $f_{+2} = 0$ for the fraction of Neon in the form of Ne^{0} and Ne^{+}, respectively (Ho & Keto 2007). Since we could not extract the star formation contribution from the [Ne III] emission lines, given the tight correlation with [O IV], we assumed that all the [Ne III] emission is coming from the AGN. Therefore, the SFR derived only from the [Ne II] represents a lower limit for the region within the extraction aperture for a fixed value of the fractional abundances for Ne^{0} and Ne^{+}. The SFR ($M_{\odot}$ yr^{-1}) values are presented in Table 1. One must note that the predicted star formation rate may depend on the aperture size, accordingly the last column of Table 1 shows the size (in kpc) that the slit samples in the dispersion direction.

We performed a K-S test analysis for the derived star formation rate for Seyfert 1 and Seyfert 2 galaxies, from this analysis we found $\sim 18.2\%$ probability of the null hypothesis, suggesting that Seyfert 1 and Seyfert 2 galaxies have statistically similar star formation rates. In this regard we found the star formation rate in Seyfert 2 galaxies to have an average of $8 \pm 2 M_{\odot}$ yr^{-1} and $7 \pm 2 M_{\odot}$ yr^{-1} for Seyfert 1 galaxies. Caution must be taken on the interpretation of the star formation rates derived from the [Ne II] luminosity. This derived SFR is a probe of the young massive stellar population and is independent of the previous star formation history. As an example, Davies et al. (2007) analysed the star formation history in the AGN dominated Seyfert 2 galaxy NGC 1068. They estimated a $SFR\,(M_{\odot}\mathrm{yr}^{-1}\ \mathrm{kpc}^{-2}) = 90 - 170$ with a starburst age of 200-300 Myr. Our results are significantly lower, $SFR\,(M_{\odot}\mathrm{yr}^{-1}\ \mathrm{kpc}^{-2}) = 0.45$, suggesting minimal current star formation, in agreement with the extensive analysis discussed by Davies et al. (2007). In general, our results are systematically lower than that found by Davies et al. (2007), given the fact that in the nuclear regions of their sample of Seyfert galaxies there appears to have been recent, 10-300 Myr, starbursts that must have already ceased. In other words, their diagnostic sample contained an older stellar population than that mapped by the [Ne II] which only traces young (< 10 Myr) stars (Leitherer et al. 1999).

6. Correlation Between the Infrared Continuum and Mid-infrared Emission Lines

Besides the low ionization mid-infrared [Ne II] emission-line, the FIR is also a good indicator of star formation, as it correlates very tightly with the 1415 MHz radio luminosity, which is thought to be produced by the same population of massive stars that heat and ionize H II regions (Condon 1992). There is a strong correlation between the FIR and [Ne II] (Sturm et al. 2002; Schweitzer et al. 2006) which supports an scenario in which the mid-infrared luminosity is dominated by the AGN, while the far-infrared luminosity is dominated by star formation (Sturm et al. 2002; Horst et al. 2006).

Figure 10 shows the correlation between the IR continuum and mid-infrared emission lines in our sample. Table 3 shows the statistical analysis for the different correlations. We found that the [Ne II] is well correlated with the continuum luminosity at 60μm, in agreement with previous studies (e.g., Sturm et al. 2002; Schweitzer et al. 2006). Compared with the [Ne II] correlation, both the [Ne III] and [O IV] show larger scatter with respect to the IR continuum (see Table 3). We have demonstrated that [Ne III] correlates with [O IV] suggesting [Ne III] as a good tracer of the AGN luminosity (see Section 4); the better correlation at shorter continuum wavelengths suggests a larger AGN contribution at those wavelengths in agreement with previous studies.

As we mentioned before, there is the technical difficulty in isolating the AGN continuum from the host galaxy emission (e.g., Lutz et al. 2004), specially in the larger field of view of *IRAS*. In order to estimate the star formation contribution in the mid- and far-infrared continuum we used the correlations between the [O IV] and the mid- and far-infrared continuum in the sources that show no PAH features in their spectra, as a template to estimate the contribution from the AGN. This contribution is inevitably mixed with some fraction of star formation in the host galaxy. By subtracting this contribution to the observed continuum luminosities we obtained the remaining fraction of star formation, e.g., a "pure" stellar component, thus, a lower limit for the star formation contribution to the mid- and far-infrared continuum.

In our sample, we found the contribution of the star formation that cannot be associated with the pure AGN sources to be: $32\pm2\%$, $45\pm5\%$, $39\pm4\%$ and $42\pm4\%$ for the luminosities at 25μm, 60μm, 100μm and FIR, respectively. These results suggest that the far-infrared continuum contains a higher fraction from a stellar component than that found in the mid-infrared (25μm). Within this sample, Seyfert 1 galaxies exhibit a narrower range of star formation contribution, $\sim 26 \pm 1\%$, to their mid- and far-infrared continuum luminosities, than that found for Seyfert 2 galaxies, $\sim 47 \pm 9\%$. Figure 11 shows the correlation between FIR and [O IV] luminosities with the percentage of star formation contribution to the FIR

luminosities indicated. The fact that most of the pure AGN sources are in the lower part of the FIR-[O IV] correlation, suggests that the fraction of star formation in the host galaxy that is mixed with the AGN contribution is minimal. Overall, these results are in good agreement from previous studies that used the infrared continuum to separate the relative contribution of star formation and nuclear activity (e.g., Shi et al. 2007) and with the values derived from the [O IV]-[Ne II] correlation, which shows that Seyfert 2 galaxies have, on average, a stronger star formation contribution.

In order to assess the relative contribution from the AGN to the mid- and far-infrared continuum within Seyfert classification, we investigated the ratio of [O IV] with the 25μm, 60μm and FIR continuum luminosities. We found that Seyfert 1 and Seyfert 2 galaxies are statistically different in their AGN contribution to their 60μm and FIR luminosities with a probability of the null hypothesis of 0.2% and 0.4%, respectively. On the other hand, the K-S test to the [O IV]/25μm ratio shows that two samples drawn from the same population would differ this much only $\sim$ 36.7% of the time.

7. Physical Conditions in the [Ne II] Emitting Region

We have established that a fraction of the [Ne II] emission must come from the AGN, given the fact that this line is present in the spectra of AGN that have no detected PAH features at 6.2μm and 11.5μm (which have been shown to be tracers of star formation activity). In order to investigate the physical conditions in the emission line regions, ionized by the AGN, for [Ne II], [Ne III], and [O IV] we generated a grid of dust-free, single-zone, constant-density models using the photoionization code CLOUDY, version 07.02.01, last described by Ferland et al. (1998). In this grid, hydrogen density (n_H) and ionization parameter U were varied. The ionization parameter U is defined as (see Osterbrock & Ferland 2006):

$$U = \frac{1}{4\pi R^2 c n_H} \int_{\nu_o}^{\infty} \frac{L_\nu}{h\nu} d\nu = \frac{Q(H)}{4\pi R^2 c n_H}, \quad (1)$$

where R is the distance to the cloud , c is the speed of light and $Q(H)$ is the flux of ionizing photons.

We used a set of roughly solar abundances (e.g., Grevesse & Anders 1989). The logs of the abundances relative to H by number are: He: -1; C: -3.46; N: -3.92; O: -3.19; Ne: -3.96; Na: -5.69; Mg: -4.48; Al: -5.53; Si: -4.50; P: -6.43; S: -4.82; Ar: -5.40; Ca: -5.64; Fe: -4.40 and Ni: -5.75. We assumed a column density of 10^{21}cm^{-2}, which is typical of the narrow line region (e.g., Kraemer et al. 2000).

Assuming a distance of R = 130 pc for the NLR (see M08), we overlaid the observed

mid-infrared emission line fluxes correlations (i.e., [Ne II]-[Ne III], [Ne II]-[O IV] and [Ne III]-[O IV]) from the "pure" AGN sources with those obtained from the photoionization modeling. From this comparison we derived the parameter space (U, n_H) required to reproduce the observed relationships within their given dispersion. The predicted, intrinsic fluxes from the photoionization models are the line fluxes emitted at the ionized face of the slab of gas, used to model the NLR. Caution must be taken when comparing [Ne II], [Ne III] and [O IV] given the fact that the observed [Ne II] fluxes can have contribution from both a star formation and AGN. In this regard, we are only interested in the AGN component of [Ne II], as deconvolved with the method presented in this work. On the other hand, the observed [Ne III] and [O IV] in our sample have been assumed to represent the AGN power.

From the observed [Ne III]/[Ne II] ratios we obtained a range in ionization parameter $-4.00 < \log(U) < -3.50$ and for the hydrogen density 4.25 (cm^{-3}) $< \log(n_H) <$ 5.50 (cm^{-3}). From the same set of models, we investigated the relationship between the AGN component of [Ne II] and [O IV] emission fluxes. From the observed range of [O IV]/[Ne II] ratios we obtained $-3.20 < \log(U) < -2.45$ and 3.25 (cm^{-3}) $< \log(n_H) <$ 4.50 (cm^{-3}). Finally, we investigated the ratios between the [O IV] and [Ne III] emission fluxes. We obtained a range for the ionization parameter, $-3.20 < \log(U) < -1.65$, and for the hydrogen density, 2.00 (cm^{-3}) $< \log(n_H) <$ 4.50 (cm^{-3}). This range in parameter space is the closest match to the one found from the [O IV]/[O III] ratio (M08), $-1.50 < \log(U) < -1.30$ and 2.0 (cm^{-3}) $< \log(n_H) <$ 4.25 (cm^{-3}).

In Figure 12 we show the allowed range in parameter space from the different emission line correlations and compared them with the parameter space obtained from the [O IV]/[O III] ratios (M08). Given the low ionization parameter obtained for [Ne II], it is possible that the [Ne II] that is produced by the AGN could originate in a more distant region that [O IV]. On the other hand, the [Ne II]-[O IV] relationship suggests a different [Ne II] component at higher ionization and lower densities than that found from the [Ne II] - [Ne III] correlation, indicating a more closer and/or compact [Ne II] emitting region. Another possibility is that [Ne II] forms in regions that are irradiated by the continuum filtered by ionized gas (Kraemer et al. 2008). However for uncovered gas, there is only a small range in parameter space where the model successfully predicts the [Ne II] emission associated with the AGN.

8. Conclusions

We have investigated the ionization state of the emission-line gas in Seyfert galaxies with the aim of constraining the active galactic nuclei (AGN) and star formation contributions in

the mid- and far-infrared spectra for a sample of 103 Seyfert galaxies. We found the ratio between the AGN power and star formation, as shown by [O IV]/[Ne II], to be smaller in Seyfert 2 than in Seyfert 1 galaxies. In this regard, we also found a correlation between [Ne III] and [O IV] versus [Ne II], with a clear separation between Seyfert groups. This separation suggests that the [Ne II] emission has two different contributions: a component that could be associated with the AGN ionizing continuum and a component produced by photoionization from star formation regions. The evidence for the former is the presence of [Ne II] in Seyfert galaxies with no detectable PAH features at 6.2 μm and 11.5 μm. We also obtained a strong correlation between [Ne III] and [O IV] confirming that [Ne III] can also be used to estimate the intrinsic power of the AGN.

We used the [O IV] and [Ne II] correlation from the sources with no detectable PAH features as a template to deconvolve the star formation and AGN contribution in the [Ne II] emission. We found that Seyfert 2 galaxies, on average, have a relatively higher star formation contribution in their [Ne II], by a factor of ~ 1.5, than Seyfert 1 galaxies, in agreement with other observations and theoretical work on circumnuclear regions of AGN (e.g., Terlevich & Melnick 1985; Heckman et al. 1989; Maiolino et al. 1997; González Delgado et al. 2001; Deo et al. 2007). Using the stellar [Ne II] luminosity as a SFR estimator we found that Seyfert 2 galaxies have similar star formation rates in their spectra, $8 \pm 2 M_{\odot}$ yr^{-1} to that found for Seyfert 1 galaxies, $7 \pm 2 M_{\odot}$ yr^{-1}. This result must be interpreted carefully given the fact that [Ne II] emission provides an instantaneous measure of the star formation rate, independent of the previous star formation history. Thus, caution most be taken when comparing with other SFR indicators on galaxies with recent starbursts, but are no longer forming massive stars, in which case our star formation predictions may account only for a small fraction of a give SFR. Overall we found that 77% of the Seyfert 2 galaxies in our sample show some star formation contribution to their [Ne II] observed luminosities while 56% of the Seyfert 1 galaxies have some stellar component.

We used the correlations between the mid- and far-infrared continuum with the [O IV] luminosities in the non-PAH sources to estimate the star formation contribution in the mid- and far-infrared continua. The resulting star formation contribution represents a lower limit given the fact that some fraction of the star formation from the host galaxy is mixed with the AGN contribution in the mid- and far-infrared continuum in our sample of pure AGN sources. Averaged over all the sample we found the contribution from star formation to the 25μm, 60μm, 100μm and FIR luminosities to be: $32 \pm 2\%$, $45 \pm 5\%$, $39 \pm 4\%$ and $42 \pm 4\%$, respectively. We also found that Seyfert 1 galaxies exhibit a narrower range of star formation contribution, $\sim 26 \pm 1\%$, to their mid- and far-infrared continuum luminosities, than that found for Seyfert 2 galaxies, $\sim 47 \pm 9\%$.

We also found a good correlation between [Ne II] and mid- and far-infrared luminosities, with the strongest correlation for the [Ne II]-60μm. This result is in agreement with previous studies that link both the FIR and [Ne II] emission with star formation. We found a weaker correlation between [O IV] and [Ne III] versus the FIR luminosities. This result suggest that part of the FIR luminosity is reprocessed photons from the AGN, most likely through reradiation of the AGN continuum by dust. Assuming that the infrared continuum is dominated by emission from dust grains, we found in our sample, that Seyfert 2 galaxies possess cooler dust, with an average $\alpha_{25-60} = -1.5 \pm 0.1$, than Seyfert 1 galaxies which have $\alpha_{25-60} = -0.8 \pm 0.1$. In agreement, we also found that Seyfert 1 and Seyfert 2 galaxies are statistically different in terms of their relative contribution from the AGN to the 60μm and FIR but have a similar contribution in the 25μm.

Summarizing, we found that Seyfert 1 and Seyfert 2 galaxies are statistically different in terms of the relative contribution from the AGN and star formation ,as showed by the [O IV]/[Ne II] ratios. From this we found that Seyfert 2 galaxies have a higher star formation contribution, relative to the strength of the AGN, than that found in Seyfert 1 galaxies but have similar star formation rates. These results suggest that the differences between Seyfert galaxies cannot be solely due to viewing angle dependence.

We would like to thank our anonymous referee for her/his suggestions that improved the paper. This research has made use of NASA's Astrophysics Data System. Also, this research has made use of the NASA/IPAC Extragalactic Database (NED) which is operated by the Jet Propulsion Laboratory, California Institute of Technology, under contract with the National Aeronautics and Space Administration. The IRS was a collaborative venture between Cornell University and Ball Aerospace Corporation funded by NASA through the Jet Propulsion Laboratory and Ames Research Center. SMART was developed by the IRS Team at Cornell University and is available through the Spitzer Science Center at Caltech. Basic research in astronomy at the NRL is supported by 6.1 base funding.

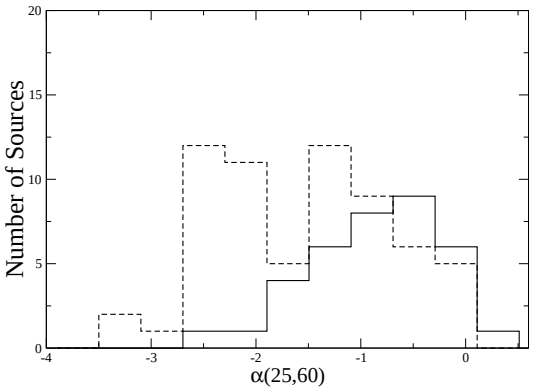

Fig. 3.— Comparison between the mid- to far-infrared index, α_{25-60}, for Seyfert 1 (*solid line*) and Seyfert 2 (*dashed line*) galaxies. This sample includes 35 Seyfert 1 and 60 Seyfert 2 galaxies. The K-S test for the spectral index returns 0.1% probability of the null hypothesis.

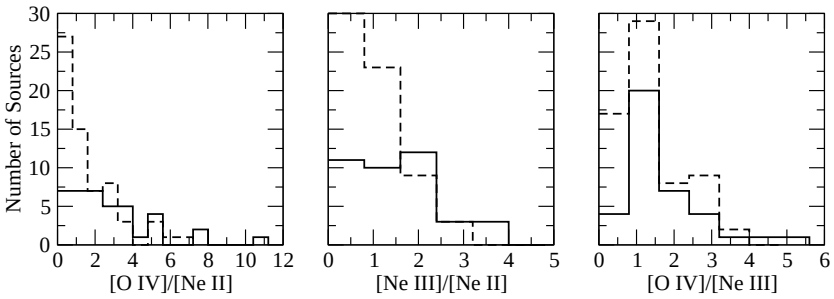

Fig. 4.— Comparison of the [O IV]/[Ne II], [Ne III]/[Ne II] and [O IV]/[Ne III] distributions in Seyfert 1 and Seyfert 2 galaxies. For the [O IV]/[Ne II], [Ne III]/[Ne II] and [O IV]/[Ne III] ratios the K-S test returns $\sim 0.9\%$, $\sim 1.1\%$ and $\sim 37.7\%$ probability of the null hypothesis, respectively.

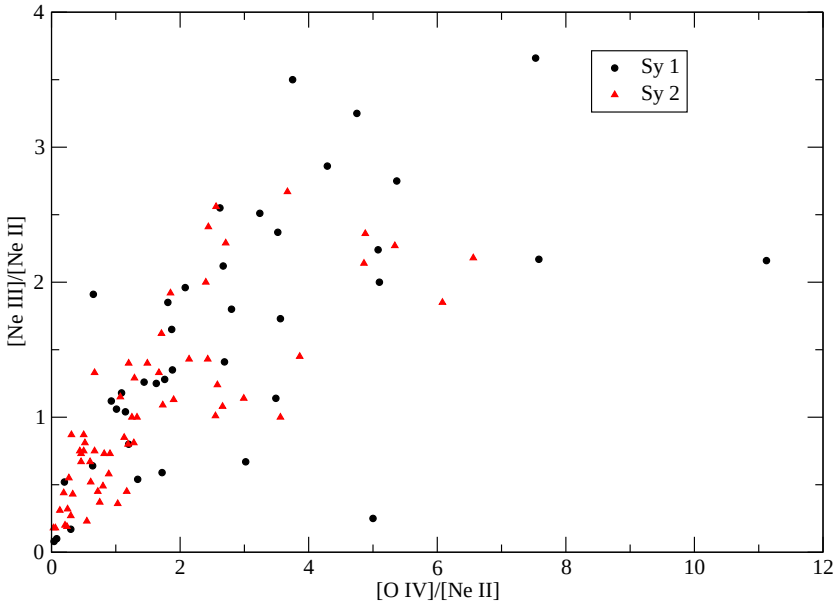

Fig. 5.— [Ne III]/[Ne II] vs. [O IV]/[Ne II] ratios in Seyfert 1 (circles) and Seyfert 2 (triangle) galaxies. Of particular interest in this comparison is that below [Ne III]/[Ne II] < 1.0 and [O IV]/[Ne II] < 2.0 there are only 9 Seyfert 1 galaxies but the majority of the Seyfert 2 galaxies ($\sim 60\%$ of the Seyfert 2 population)

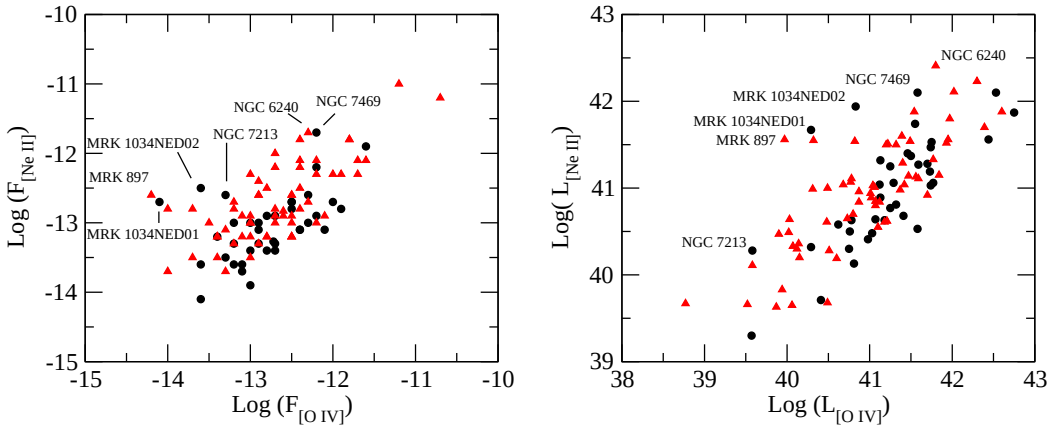

Fig. 6.— Correlation between [Ne II] versus [O IV] fluxes and luminosities. The identified sources are known to have strong star formation activity. Symbols are identical to those in Figure 5.

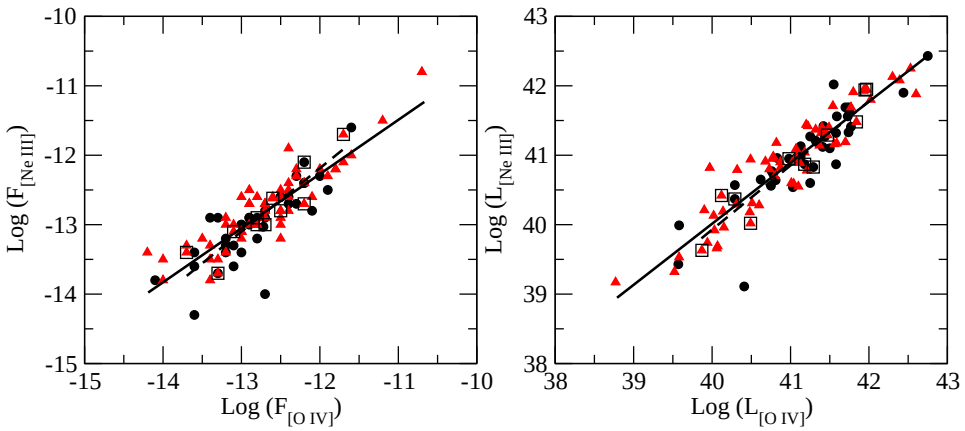

Fig. 7.— Correlation between [Ne III] and [O IV] fluxes, and luminosities. The squares represent AGN with no detectable PAH features at 6.2 μm and 11.5 μm. The *solid line* represents the linear fit obtained for the full sample and the *dashed line* represents the linear fit for the pure AGN sources. Symbols are identical to those in Figure 5.

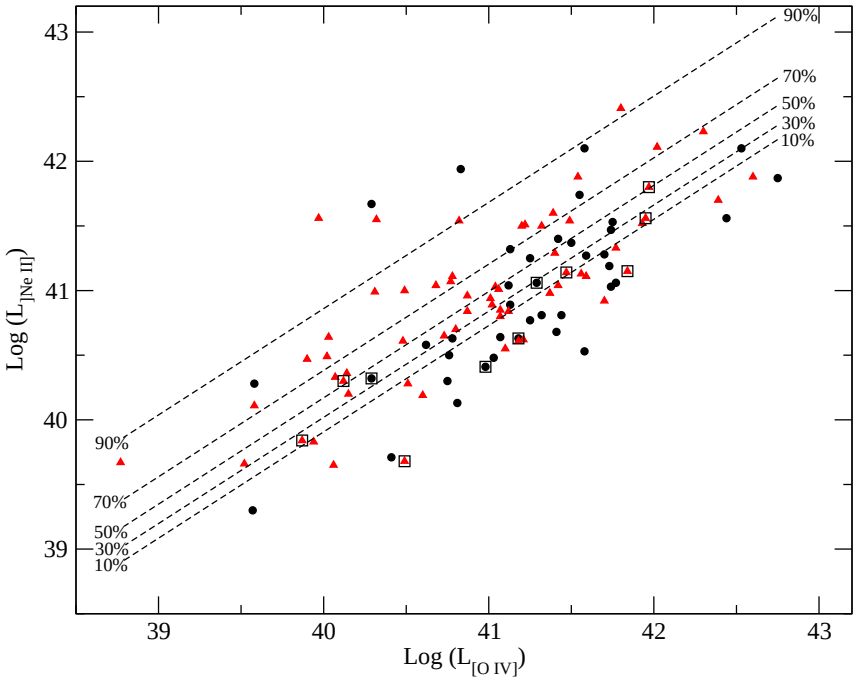

Fig. 8.— Correlation between [Ne II] and [O IV] luminosities. The *dashed lines* represent the percentage of stellar component in the [Ne II] emission line, based on the predicted AGN contribution. The squares represent AGN with no detectable PAH features at 6.2 μm and 11.5 μm. Symbols are identical to those in Figure 5.

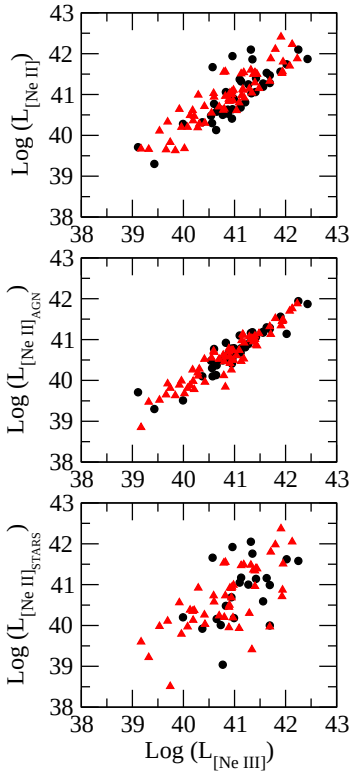

Fig. 9.— Correlation between [Ne II] and [Ne III] after the deconvolution of the AGN and stellar component in the observed [Ne II] luminosities. In the upper, middle and lower panel we present the observed (AGN+stellar component), AGN and the stellar component for [Ne II] versus [Ne III] emission line luminosities. Symbols are identical to those in Figure 5.

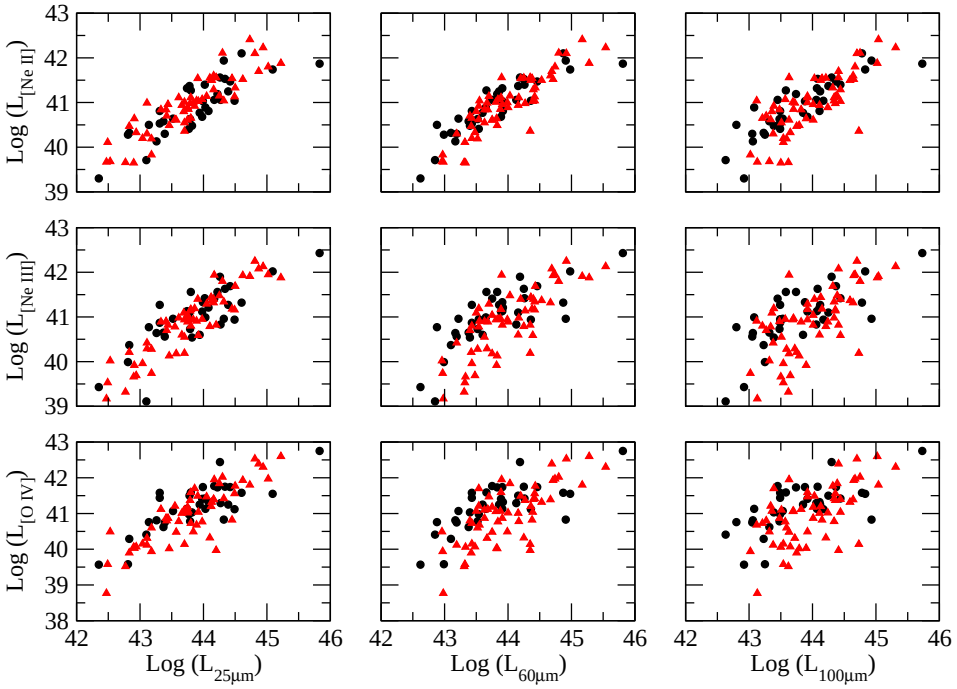

Fig. 10.— Correlation between the IR continuum and mid-infrared emission line luminosities. The statistical analysis for the different correlations between the mid-infrared emission lines and mid- and far-infrared continuum are presented in Table 3. Symbols are identical to those in Figure 5.

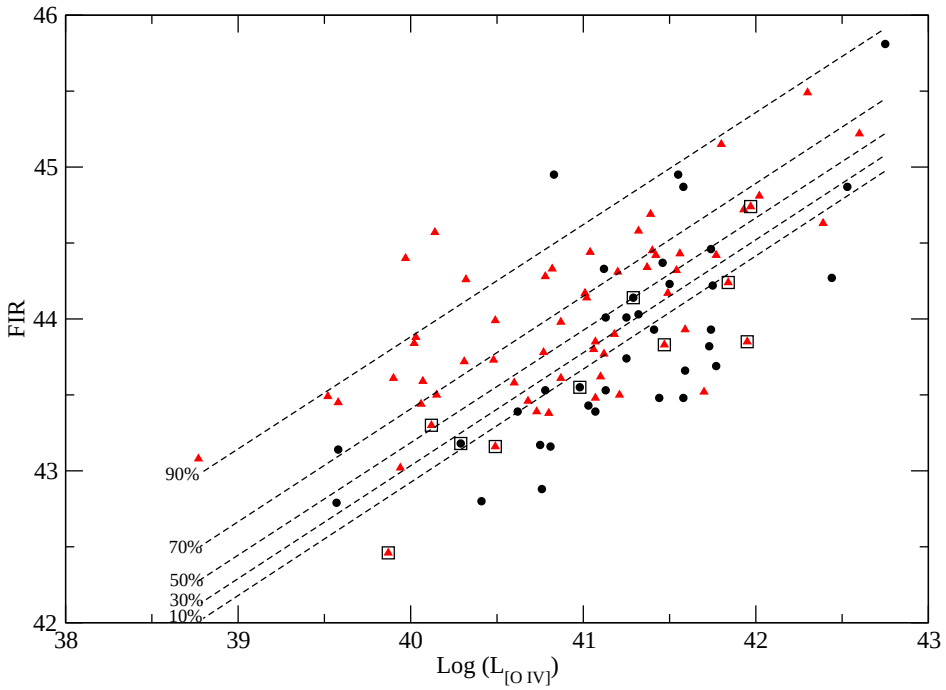

Fig. 11.— Correlation between the FIR luminosities and [O IV]. The *dashed lines* represent the percentage of "pure" stellar component in the FIR, based on the combined AGN+host galaxy stellar contribution. The squares represent the pure AGN sources, i.e., no detectable PAH features at 6.2μm and 11.2μm. Symbols are identical to those in Figure 5.

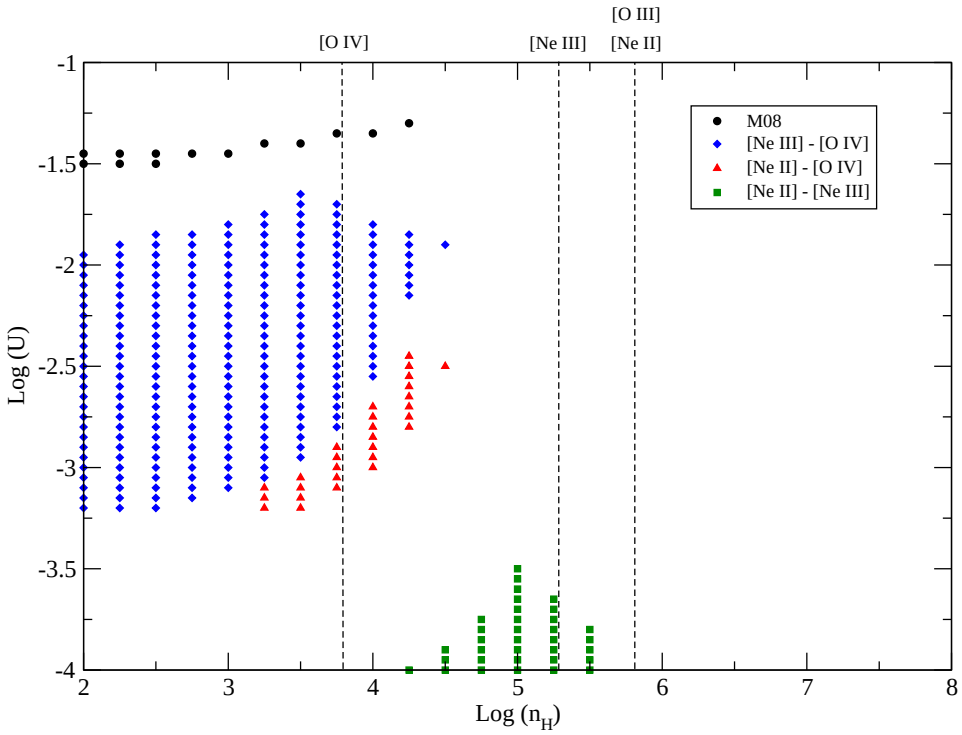

Fig. 12.— Comparison between the parameter space required for the different mid-infrared line relationships. The dashed lines represent the critical density for the different emission lines.

REFERENCES

Abel, N. P., & Satyapal, S. 2008, ApJ, 678, 686

Antonucci, R. 1993, ARA&A, 31, 473

Antonucci, R. R. J., & Miller, J. S. 1985, ApJ, 297, 621

Armus, L., Charmandaris, V., Bernard-Salas, J., Spoon, H. W. W., Marshall, J. A., Higdon, S. J. U., Desai, V., Teplitz, H. I., Hao, L., Devost, D., Brandl, B. R., Wu, Y., Sloan, G. C., Soifer, B. T., Houck, J. R., & Herter, T. L. 2007, ApJ, 656, 148

Bevington, P. R., & Robinson, D. K. 2003, Data reduction and error analysis for the physical sciences (Data reduction and error analysis for the physical sciences, 3rd ed., by Philip R. Bevington, and Keith D. Robinson. Boston, MA: McGraw-Hill, ISBN 0-07-247227-8, 2003.)

Buchanan, C. L., Gallimore, J. F., O'Dea, C. P., Baum, S. A., Axon, D. J., Robinson, A., Elitzur, M., & Elvis, M. 2006, AJ, 132, 401

Calzetti, D., Kennicutt, Jr., R. C., Bianchi, L., Thilker, D. A., Dale, D. A., Engelbracht, C. W., Leitherer, C., Meyer, M. J., Sosey, M. L., Mutchler, M., Regan, M. W., Thornley, M. D., Armus, L., Bendo, G. J., Boissier, S., Boselli, A., Draine, B. T., Gordon, K. D., Helou, G., Hollenbach, D. J., Kewley, L., Madore, B. F., Martin, D. C., Murphy, E. J., Rieke, G. H., Rieke, M. J., Roussel, H., Sheth, K., Smith, J. D., Walter, F., White, B. A., Yi, S., Scoville, N. Z., Polletta, M., & Lindler, D. 2005, ApJ, 633, 871

Cid Fernandes, R., Gu, Q., Melnick, J., Terlevich, E., Terlevich, R., Kunth, D., Rodrigues Lacerda, R., & Joguet, B. 2004, MNRAS, 355, 273

Cid Fernandes, R., Heckman, T., Schmitt, H., Delgado, R. M. G., & Storchi-Bergmann, T. 2001, ApJ, 558, 81

Cid Fernandes, R. J., & Terlevich, R. 1995, MNRAS, 272, 423

Clavel, J., Schulz, B., Altieri, B., Barr, P., Claes, P., Heras, A., Leech, K., Metcalfe, L., & Salama, A. 2000, A&A, 357, 839

Condon, J. J. 1992, ARA&A, 30, 575

Dale, D. A., Smith, J. D. T., Armus, L., Buckalew, B. A., Helou, G., Kennicutt, Jr., R. C., Moustakas, J., Roussel, H., Sheth, K., Bendo, G. J., Calzetti, D., Draine, B. T., Engelbracht, C. W., Gordon, K. D., Hollenbach, D. J., Jarrett, T. H., Kewley, L. J., Leitherer, C., Li, A., Malhotra, S., Murphy, E. J., & Walter, F. 2006, ApJ, 646, 161

Davies, R. I., Mueller Sánchez, F., Genzel, R., Tacconi, L. J., Hicks, E. K. S., Friedrich, S., & Sternberg, A. 2007, ApJ, 671, 1388

Deo, R. P., Crenshaw, D. M., Kraemer, S. B., Dietrich, M., Elitzur, M., Teplitz, H., & Turner, T. J. 2007, ApJ, 671, 124

Ferland, G. J., Korista, K. T., Verner, D. A., Ferguson, J. W., Kingdon, J. B., & Verner, E. M. 1998, PASP, 110, 761

Förster Schreiber, N. M., Roussel, H., Sauvage, M., & Charmandaris, V. 2004, A&A, 419, 501

Genzel, R., Lutz, D., Sturm, E., Egami, E., Kunze, D., Moorwood, A. F. M., Rigopoulou, D., Spoon, H. W. W., Sternberg, A., Tacconi-Garman, L. E., Tacconi, L., & Thatte, N. 1998, ApJ, 498, 579

González Delgado, R. M., Heckman, T., & Leitherer, C. 2001, ApJ, 546, 845

Gorjian, V., Cleary, K., Werner, M. W., & Lawrence, C. R. 2007, ApJ, 655, L73

Grevesse, N., & Anders, E. 1989, in American Institute of Physics Conference Series, Vol. 183, Cosmic Abundances of Matter, ed. C. J. Waddington, 1–8

Gu, Q., Melnick, J., Fernandes, R. C., Kunth, D., Terlevich, E., & Terlevich, R. 2006, MNRAS, 366, 480

Heckman, T. M., Blitz, L., Wilson, A. S., Armus, L., & Miley, G. K. 1989, ApJ, 342, 735

Heisler, C. A., Lumsden, S. L., & Bailey, J. A. 1997, Nature, 385, 700

Ho, L. C., Filippenko, A. V., & Sargent, W. L. W. 2003, ApJ, 583, 159

Ho, L. C., & Keto, E. 2007, ApJ, 658, 314

Horst, H., Smette, A., Gandhi, P., & Duschl, W. J. 2006, A&A, 457, L17

Houck, J. R., Roellig, T. L., van Cleve, J., Forrest, W. J., Herter, T., Lawrence, C. R., Matthews, K., Reitsema, H. J., Soifer, B. T., Watson, D. M., Weedman, D., Huisjen, M., Troeltzsch, J., Barry, D. J., Bernard-Salas, J., Blacken, C. E., Brandl, B. R., Charmandaris, V., Devost, D., Gull, G. E., Hall, P., Henderson, C. P., Higdon, S. J. U., Pirger, B. E., Schoenwald, J., Sloan, G. C., Uchida, K. I., Appleton, P. N., Armus, L., Burgdorf, M. J., Fajardo-Acosta, S. B., Grillmair, C. J., Ingalls, J. G., Morris, P. W., & Teplitz, H. I. 2004, ApJS, 154, 18

Kennicutt, Jr., R. C. 1998, ARA&A, 36, 189

Khachikian, E. Y., & Weedman, D. W. 1974, ApJ, 192, 581

Kraemer, S. B., Crenshaw, D. M., Hutchings, J. B., Gull, T. R., Kaiser, M. E., Nelson, C. H., & Weistrop, D. 2000, ApJ, 531, 278

Kraemer, S. B., Schmitt, H. R., & Crenshaw, D. M. 2008, ApJ, 679, 1128

Leitherer, C., Schaerer, D., Goldader, J. D., Delgado, R. M. G., Robert, C., Kune, D. F., de Mello, D. F., Devost, D., & Heckman, T. M. 1999, ApJS, 123, 3

Low, F. J., Young, E., Beintema, D. A., Gautier, T. N., Beichman, C. A., Aumann, H. H., Gillett, F. C., Neugebauer, G., Boggess, N., & Emerson, J. P. 1984, ApJ, 278, L19

Lutz, D., Genzel, R., Sternberg, A., Netzer, H., Kunze, D., Rigopoulou, D., Sturm, E., Egami, E., Feuchtgruber, H., Moorwood, A. F. M., & de Graauw, T. 1996, A&A, 315, L137

Lutz, D., Maiolino, R., Spoon, H. W. W., & Moorwood, A. F. M. 2004, A&A, 418, 465

Maiolino, R., Krabbe, A., Thatte, N., & Genzel, R. 1998, ApJ, 493, 650

Maiolino, R., Ruiz, M., Rieke, G. H., & Papadopoulos, P. 1997, ApJ, 485, 552

Markwardt, C. B., Tueller, J., Skinner, G. K., Gehrels, N., Barthelmy, S. D., & Mushotzky, R. F. 2005, ApJ, 633, L77

Meléndez, M., Kraemer, S. B., Armentrout, B. K., Deo, R. P., Crenshaw, D. M., Schmitt, H. R., Mushotzky, R. F., Tueller, J., Markwardt, C. B., & Winter, L. 2008, ArXiv e-prints, 804

Moshir, M., Kopan, G., Conrow, T., McCallon, H., Hacking, P., Gregorich, D., Rohrbach, G., Melnyk, M., Rice, W., Fullmer, L., White, J., & Chester, T. 1990, in Bulletin of the American Astronomical Society, Vol. 22, Bulletin of the American Astronomical Society, 1325–+

Neugebauer, G., Habing, H. J., van Duinen, R., Aumann, H. H., Baud, B., Beichman, C. A., Beintema, D. A., Boggess, N., Clegg, P. E., de Jong, T., Emerson, J. P., Gautier, T. N., Gillett, F. C., Harris, S., Hauser, M. G., Houck, J. R., Jennings, R. E., Low, F. J., Marsden, P. L., Miley, G., Olnon, F. M., Pottasch, S. R., Raimond, E., Rowan-Robinson, M., Soifer, B. T., Walker, R. G., Wesselius, P. R., & Young, E. 1984, ApJ, 278, L1

Osterbrock, D. E., & Ferland, G. J. 2006, Astrophysics of gaseous nebulae and active galactic nuclei (Astrophysics of gaseous nebulae and active galactic nuclei, 2nd. ed. by D.E. Osterbrock and G.J. Ferland. Sausalito, CA: University Science Books, 2006)

Perez-Olea, D. E., & Colina, L. 1996, ApJ, 468, 191

Peterson, B. M., Ferrarese, L., Gilbert, K. M., Kaspi, S., Malkan, M. A., Maoz, D., Merritt, D., Netzer, H., Onken, C. A., Pogge, R. W., Vestergaard, M., & Wandel, A. 2004, ApJ, 613, 682

Peterson, B. M., & Wandel, A. 2000, ApJ, 540, L13

Pier, E. A., & Krolik, J. H. 1992, ApJ, 401, 99

Press, W. H., Teukolsky, S. A., Vetterling, W. T., & Flannery, B. P. 1992, Numerical recipes in FORTRAN. The art of scientific computing (Cambridge: University Press, —c1992, 2nd ed.)

Rees, M. J. 1984, ARA&A, 22, 471

Sanders, D. B., Mazzarella, J. M., Kim, D.-C., Surace, J. A., & Soifer, B. T. 2003, AJ, 126, 1607

Sanders, D. B., & Mirabel, I. F. 1996, ARA&A, 34, 749

Sanders, D. B., Soifer, B. T., Elias, J. H., Neugebauer, G., & Matthews, K. 1988, ApJ, 328, L35

Schmitt, H. R., Antonucci, R. R. J., Ulvestad, J. S., Kinney, A. L., Clarke, C. J., & Pringle, J. E. 2001, ApJ, 555, 663

Schmitt, H. R., Storchi-Bergmann, T., & Fernandes, R. C. 1999, MNRAS, 303, 173

Schweitzer, M., Lutz, D., Sturm, E., Contursi, A., Tacconi, L. J., Lehnert, M. D., Dasyra, K. M., Genzel, R., Veilleux, S., Rupke, D., Kim, D.-C., Baker, A. J., Netzer, H., Sternberg, A., Mazzarella, J., & Lord, S. 2006, ApJ, 649, 79

Shi, Y., Ogle, P., Rieke, G. H., Antonucci, R., Hines, D. C., Smith, P. S., Low, F. J., Bouwman, J., & Willmer, C. 2007, ApJ, 669, 841

Soifer, B. T., Boehmer, L., Neugebauer, G., & Sanders, D. B. 1989, AJ, 98, 766

Spinoglio, L., Malkan, M. A., Rush, B., Carrasco, L., & Recillas-Cruz, E. 1995, ApJ, 453, 616

Sturm, E., Lutz, D., Verma, A., Netzer, H., Sternberg, A., Moorwood, A. F. M., Oliva, E., & Genzel, R. 2002, A&A, 393, 821

Terlevich, E., Diaz, A. I., & Terlevich, R. 1990, MNRAS, 242, 271

Terlevich, R., & Melnick, J. 1985, MNRAS, 213, 841

Tommasin, S., Spinoglio, L., Malkan, M. A., Smith, H., González-Alfonso, E., & Charmandaris, V. 2008, ApJ, 676, 836

Weedman, D. W., Hao, L., Higdon, S. J. U., Devost, D., Wu, Y., Charmandaris, V., Brandl, B., Bass, E., & Houck, J. R. 2005, ApJ, 633, 706

Table 1. The Infrared Sample of Seyfert Galaxies

Name	Type	z	$\log L_{25\mu m}$	$\log L_{60\mu m}$	$\log L_{FIR}$	$\log L_{[Ne\ II]}$ (ergs s^{-1})	$\log L_{[Ne\ III]}$	$\log L_{[O\ IV]}$	SC (%)	SFR ($M_\odot\ yr^{-1}$)	Aperture (kpc)	Reference
3C120	1	0.033010	44.26	44.19	44.27	41.56	41.90	42.44	0	0	3.23	1
3C273	1	0.158339	45.83	45.81	45.81	41.87	42.43	42.75	0	0	16.45	1
3C382	1	0.057870	43.94	43.60	43.74	40.77	40.60	41.25	0	0	5.73	1
3C390.3	1	0.056100	44.39	43.86	44.01	41.25	41.27	41.25	56.11	5.77	5.55	1
3C452	2	0.081100	...	...	...	41.51	41.42	41.22	77.13	14.39	8.12	1
CGCG381-051	2	0.030668	44.10	44.25	44.26	41.55	40.79	40.32	96.24	19.61	2.36	2
Circinus	2	0.001448	43.57	43.75	43.73	40.61	40.18	40.48	55.00	1.28	0.14	4
Cen A	2	0.001825	43.17	43.76	43.82	40.20	40.08	39.93	59.27	0.54	0.18	5
ESO012-G021	1	0.030021	43.78	44.16	44.23	41.37	41.10	41.50	47.42	6.50	2.93	3
ESO103-G035	1	0.013286	44.03	43.65	43.53	40.89	40.99	41.13	19.60	0.87	1.29	1
ESO141-G055	1	0.036000	44.08	43.92	44.03	40.81	41.21	41.32	0	0	3.53	3
ESO541-IG012	2	0.056552	44.49	44.42	44.43	41.13	41.16	41.56	0	0	5.6	3
ESO545-G013	1	0.033730	44.02	44.26	44.37	41.40	41.42	41.46	54.13	7.91	3.3	3
F01475-0740	2	0.017666	43.89	43.55	43.46	41.04	40.91	40.68	75.89	4.77	1.31	2
F04385-0828	2	0.015100	43.98	43.84	43.78	41.07	40.95	40.77	73.51	5.05	1.12	2
F15480-0344	2	0.030300	44.25	44.03	44.24	41.15	41.48	41.84	0	0	2.27	2
I Zw 1	1	0.061142	45.09	44.98	44.95	41.74	42.02	41.55	75.00	23.92	18.07	4
I Zw 92	2	0.037800	44.29	44.32	44.32	41.88	41.71	41.54	82.28	36.21	11.05	4
IC4329a	1.2	0.016054	44.17	43.75	43.69	41.06	41.41	41.77	0	0	1.56	1
IRAS00198-7926	2	0.072800	45.22	45.28	45.22	41.88	42.23	42.60	0	0	7.26	3
IRAS00521-7054	2	0.068900	45.02	44.74	44.74	41.80	41.95	41.97	51.75	18.85	6.86	3
IRASF15091-2107	1	0.044607	44.42	44.53	44.49	41.71	41.86	42.14	18.47	5.47	4.39	3
IRASF22017+0319	2	0.061100	44.87	44.69	44.63	41.70	42.08	42.39	0	0	6.06	3
MCG-2-40-4	2	0.025194	44.16	44.40	44.45	41.29	41.40	41.40	47.28	5.32	1.88	2
MCG-2-58-22	1.5	0.046860	...	...	...	41.28	41.69	41.70	5.19	0.58	4.62	1
MCG-2-8-39	2	0.029894	44.05	43.70	43.83	41.14	41.29	41.47	14.66	1.17	2.24	2
MCG-3-58-7	2	0.031462	44.32	44.42	44.42	41.04	41.34	41.42	2.37	0.15	2.36	2
MCG-5-13-17	1.5	0.012642	43.37	43.38	43.39	40.58	40.65	40.62	38.41	0.85	0.94	2
MCG-6-30-15	1.2	0.007749	43.10	42.85	42.80	39.71	39.11	40.41	0	0	0.57	2
MRK 1034NED01	1	0.033633	44.32	44.91	44.95	41.94	40.96	40.83	96.03	48.58	3.29	3
MRK 1034NED02	1	0.033710	...	...	...	41.67	40.57	40.29	97.33	26.41	3.3	3
MRK 231	1	0.04217	45.61	45.80	45.75	41.86	41.35	41.60	79.43	33.68	4.15	5
MRK 273	2	0.037780	44.94	45.54	45.49	42.23	42.13	42.30	66.28	64.93	11.04	4

Table 1—Continued

Name	Type	z	$\log L_{25\mu m}$	$\log L_{60\mu m}$	$\log L_{FIR}$	$\log L_{[Ne\ II]}$ (ergs s^{-1})	$\log L_{[Ne\ III]}$	$\log L_{[O\ IV]}$	SC (%)	SFR ($M_\odot\ yr^{-1}$)	Aperture (kpc)	Reference
MRK 3	2	0.014000	44.17	43.90	43.85	41.56	41.94	41.95	20.13	4.25	1.04	2
MRK 334	1.8	0.021945	44.12	44.36	44.31	41.50	41.44	41.20	77.74	14.19	1.64	2
MRK 335	1.2	0.025785	43.82	43.40	43.43	40.48	40.54	41.03	0	0	2.51	1
MRK 348	2	0.015034	43.69	43.50	43.48	40.80	41.09	41.07	13.41	0.49	1.12	2
MRK 471	1.8	0.034234	43.75	44.00	44.14	40.89	40.89	41.02	36.03	1.62	2.57	2
MRK 509	1.2	0.034397	44.34	44.25	44.22	41.53	41.63	41.75	42.16	8.36	3.37	1
MRK 573	2	0.017179	43.86	43.54	43.52	40.92	41.19	41.70	0	0	4.97	4
MRK 6	1.5	0.018813	43.80	43.66	43.66	41.27	41.56	41.59	20.88	2.23	1.4	2
MRK 609	1.8	0.034488	44.13	44.53	44.58	41.50	41.37	41.32	71.80	13.11	2.59	2
MRK 622	2	0.023229	43.76	43.88	43.85	40.85	40.97	41.07	21.87	0.90	1.73	2
MRK 79	1.2	0.022189	43.99	43.91	43.93	41.03	41.33	41.74	0	0	1.65	2
MRK 817	1.5	0.031455	44.49	44.36	44.33	41.04	40.94	41.12	44.77	2.82	2.36	2
MRK 883	1.9	0.037496	43.91	44.20	44.17	41.54	41.40	41.49	64.15	12.73	2.82	2
MRK 897	2	0.026340	44.20	44.35	44.40	41.56	40.82	39.97	98.10	20.75	2.57	3
MRK 9	1.5	0.039874	44.27	44.13	44.14	41.06	40.83	41.29	26.41	1.74	3.92	3
NGC 1068	2	0.003793	44.50	44.43	44.42	41.33	41.69	41.77	4.34	0.54	1.09	4
NGC 1125	2	0.010931	43.41	43.63	43.61	40.84	40.90	40.87	45.40	1.83	0.81	2
NGC 1194	1	0.013596	43.39	43.19	43.17	40.30	40.56	40.75	0	0	1.01	2
NGC 1275	2	0.017559	44.45	44.38	44.33	41.51	41.13	40.74	90.86	16.92	1.71	5
NGC 1320	2	0.013515	43.70	43.63	43.62	40.55	40.55	41.10	0	0	1	2
NGC 1365	1.8	0.005457	43.92	44.39	44.44	41.03	40.59	41.04	51.09	3.14	0.53	1
NGC 1667	2	0.015167	43.61	44.17	44.28	41.11	40.98	40.78	75.59	5.67	1.13	2
NGC 2639	1.9	0.011128	42.83	43.42	43.61	40.47	40.21	39.90	79.37	1.35	0.83	2
NGC 2992	2	0.007710	43.33	43.68	43.77	40.84	40.89	41.12	12.90	0.52	0.75	1
NGC 3079	2	0.003723	42.91	43.82	43.88	40.64	39.92	40.03	82.52	2.10	0.28	2
NGC 3227	1.5	0.003859	42.83	43.10	43.18	40.32	40.37	40.29	39.90	0.48	0.29	1
NGC 3516	1.5	0.008836	43.26	43.17	43.16	40.13	40.64	40.81	0	0	0.65	2
NGC 3660	2	0.012285	42.94	43.48	43.59	40.33	39.69	40.07	60.83	0.75	1.19	3
NGC 3783	1.5	0.009730	43.79	43.52	43.53	40.63	40.73	40.78	24.23	0.59	0.94	1
NGC 3786	1.8	0.008933	...	...	...	40.28	40.31	40.51	0	0	0.66	2
NGC 3982	2	0.003699	42.47	42.98	43.08	39.67	39.17	38.77	84.94	0.23	0.27	2
NGC 4051	1.5	0.002336	42.35	42.62	42.79	39.30	39.43	39.57	0	0	0.17	2
NGC 4151	1.5	0.003319	43.14	42.88	42.88	40.50	40.77	40.76	3.42	0.06	0.25	2

Table 1—Continued

Name	Type	z	$\log L_{25\mu m}$	$\log L_{60\mu m}$	$\log L_{FIR}$	$\log L_{[Ne\ II]}$ (ergs s^{-1})	$\log L_{[Ne\ III]}$	$\log L_{[O\ IV]}$	SC (%)	SFR ($M_\odot\ yr^{-1}$)	Aperture (kpc)	Reference
NGC 424	2	0.011764	43.80	43.43	43.39	40.65	40.80	40.73	35.32	0.92	0.87	2
NGC 4388	2	0.008419	43.80	43.89	43.93	41.11	41.17	41.59	0	0	0.81	1
NGC 4501	2	0.007609	43.28	44.93	44.15	39.94	39.77	39.72	50.98	0.26	0.74	3
NGC 4507	1.9	0.011801	43.70	43.81	43.80	41.01	40.94	41.06	46.83	2.76	1.14	1
NGC 4748	1	0.014630	43.31	43.43	43.48	40.53	40.87	41.58	0	0	1.42	3
NGC 4941	2	0.003696	42.27	42.30	42.46	39.63	39.84	39.87	0	0	0.36	1
NGC 4968	2	0.009863	43.42	43.40	43.38	40.70	40.70	40.80	34.47	1.00	0.73	2
NGC 5005	2	0.003156	42.49	43.32	43.45	40.11	39.53	39.58	74.13	0.55	0.23	2
NGC 513	2	0.019544	43.44	43.91	43.98	40.96	40.82	40.87	58.41	3.09	1.46	2
NGC 5256	2	0.027863	44.30	44.80	44.81	42.11	41.80	42.02	74.46	55.83	2.08	2
NGC 526A	1.5	0.019097	...	...	...	40.63	40.87	41.18	0	0	1.86	1
NGC 5347	2	0.007789	43.18	42.97	43.02	39.83	39.74	39.94	4.73	0.02	0.75	1
NGC 5506	1.9	0.006181	43.55	43.54	43.50	40.62	40.78	41.21	0	0	0.6	1
NGC 5548	1.5	0.017175	43.77	43.54	43.55	40.41	40.95	40.98	0	0	1.28	2
NGC 5643	2	0.003999	43.18	43.52	43.58	40.19	40.28	40.60	0	0	1.15	1
NGC 5929	2	0.008312	43.46	43.83	43.84	40.49	40.13	40.02	75.93	1.37	0.62	2
NGC 5953	2	0.006555	43.11	43.67	43.72	40.99	40.29	40.31	86.57	4.86	0.48	2
NGC 6240	2	0.024480	44.73	45.17	45.15	42.41	41.91	41.80	91.42	134.62	2.39	1
NGC 6300	2	0.003699	42.90	43.33	43.44	39.65	39.66	40.06	0	0	0.36	1
NGC 6890	2	0.008069	43.04	43.43	43.50	40.20	39.96	40.15	39.01	0.36	0.78	3
NGC 7130	2	0.016151	44.16	44.67	44.69	41.60	41.32	41.39	75.04	17.46	1.2	2
NGC 7172	2	0.008683	43.17	43.67	43.74	40.71	40.41	40.80	35.54	1.05	0.84	1
NGC 7213	1.5	0.005839	42.81	42.99	43.14	40.28	39.99	39.58	82.88	0.91	0.56	1
NGC 7314	1.9	0.004763	42.53	42.96	43.16	39.68	40.02	40.49	0	0	0.46	1
NGC 7469	1.5	0.016317	44.60	44.87	44.87	42.10	41.32	41.58	88.55	64.57	1.58	1
NGC 7582	2	0.005254	43.66	44.16	44.17	40.94	40.60	41.01	43.66	2.22	0.39	1
NGC 7590	2	0.005255	42.77	43.31	43.49	39.66	39.32	39.52	36.31	0.10	0.51	3
NGC 7603	1.5	0.029524	43.74	43.91	44.01	41.32	41.13	41.13	70.85	8.65	2.21	2
NGC 7674	2	0.028924	44.62	44.71	44.72	41.52	41.93	41.93	15.63	2.99	2.16	2
NGC 931	1.5	0.016652	43.98	43.89	43.93	40.68	41.12	41.41	0	0	1.24	2
NGC 985	1	0.043143	44.42	44.46	44.46	41.47	41.69	41.74	33.49	5.72	4.24	1
PG1501+106	1.5	0.036420	44.22	43.83	43.82	41.19	41.56	41.73	0	0	3.57	1
PG1534+580	1	0.029577	43.52	43.22	43.39	40.64	40.96	41.07	0	0	2.21	1

Table 1—Continued

Name	Type	z	$\log L_{25\mu m}$	$\log L_{60\mu m}$	$\log L_{FIR}$	$\log L_{[Ne\ II]}$ (ergs s^{-1})	$\log L_{[Ne\ III]}$	$\log L_{[O\ IV]}$	SC (%)	SFR ($M_\odot\ yr^{-1}$)	Aperture (kpc)	Reference
TOL1238-364	2	0.010924	43.84	43.99	43.99	41.00	40.94	40.49	81.70	4.75	0.81	2
UGC 12138	1.8	0.024974	43.75	43.75	43.90	40.61	41.04	41.18	0	0	1.86	2
UGC 7064	1.9	0.024997	43.79	44.27	44.34	40.98	41.14	41.37	0	0	1.87	2
UM 146	1.9	0.017405	43.11	43.19	43.30	40.30	40.42	40.12	53.83	0.62	1.29	2

Note. — The sources that shows no detectable PAH features at 6.2 μm and 11.5 μm in their spectra are: F15480-0344, IRAS00521-7054, MCG-2-8-39, MRK 3, MRK 9, NGC 3227, NGC 4941, NGC 526A, NGC 5548, NGC 7314 and UM 146. The luminosities were calculated from the fluxes using $H_o = 71 kms^{-1}Mpc^{-1}$ and a deceleration parameter $q_o = 0$ with redshift values taken from NED. The last four columns show the percentage of stellar contribution to the [Ne II] emission-line (SC); the star formation rates (SFR) derived from the stellar component of [Ne II]; the aperture size in the dispersion direction (in kpc) and the last column shows the references from which the emission line fluxes were obtained. Mid- and far-infrared continuum fluxes at 25μm, 60μm and 100μm are from the *IRAS* (Soifer et al. 1989; Moshir et al. 1990; Sanders et al. 2003).

References. — (1) Present calculations, (2)Deo et al. (2007), (3)Tommasin et al. (2008), (4)Sturm et al. (2002), (5)Weedman et al. (2005)

Table 2. Statistical Analysis Between Seyfert 1 and Seyfert 2 Galaxies

	Seyfert 1			Seyfert 2			
	Measurements Available	Mean	Standard Deviation	Measurements Available	Mean	Standard Deviation	P_{K-S} (%)
$L_{[Ne\ II]}$	39	41.0	0.1	64	40.9	0.1	79.0
$L_{[Ne\ III]}$	39	41.0	0.1	64	40.9	0.1	22.8
$L_{[O\ IV]}$	39	41.2	0.1	64	40.9	0.1	10.0
$L_{25\mu m}$	36	44.0	0.1	62	43.7	0.1	27.3
$L_{60\mu m}$	36	44.0	0.1	62	44.0	0.1	70.4
$L_{100\mu m}$	36	43.9	0.1	62	44.0	0.1	29.4
$L_{FIR\mu m}$	36	43.9	0.1	62	44.0	0.1	51.3
[O IV]/[Ne II]	39	2.7	0.4	64	1.6	0.2	0.9
[Ne III]/[Ne II]	39	1.5	0.1	64	1.03	0.08	1.1
[O IV]/[Ne III]	39	2.1	0.5	64	1.4	0.1	37.7
[O IV]/$F_{25\mu m}$ (10^{-3})	36	3.1	0.6	62	2.2	0.2	36.7
[O IV]/$F_{60\mu m}$ (10^{-3})	36	3.9	0.7	62	1.8	0.3	0.2
[O IV]/FIR (10^{-3})	36	3.1	0.6	62	1.1	0.3	0.4
b/a	33	0.72	0.04	58	0.67	0.03	26.6
$\alpha_{25-60\mu m}$	36	-0.8	0.1	62	-1.5	0.1	0.1
$SC_{[Ne\ II]}$(%)	39	28	5	64	43	4	4.4
$SFR_{[Ne\ II]}(M_\odot\ yr^{-1})$	39	7	2	64	8	2	18.2

Note. — The last column, P_{K-S}, represents the Kolmogorov-Smirnov (K-S) test null probability

Table 3. Statistical Analysis for the Different Relationships Between the Mid-infrared Emission Lines and Mid- and Far-infrared Continuum for the Sample

log – log	Flux	Luminosity
[Ne II]-[Ne III]	$r_s = 0.765$	$r_s = 0.853$
[Ne II]-[O IV]	$r_s = 0.557$	$r_s = 0.729$
[Ne III]-[O IV]	$r_s = 0.878$	$r_s = 0.916$
$L_{25\mu\mathrm{m}}$-[Ne II]		$r_s = 0.883$
$L_{60\mu\mathrm{m}}$-[Ne II]		$r_s = 0.885$
$L_{100\mu\mathrm{m}}$-[Ne II]		$r_s = 0.796$
L_{FIR}-[Ne II]		$r_s = 0.856$
$L_{25\mu\mathrm{m}}$-[Ne III]		$r_s = 0.867$
$L_{60\mu\mathrm{m}}$-[Ne III]		$r_s = 0.765$
$L_{100\mu\mathrm{m}}$-[Ne III]		$r_s = 0.663$
L_{FIR}-[Ne III]		$r_s = 0.732$
$L_{25\mu\mathrm{m}}$-[O IV]		$r_s = 0.809$
$L_{60\mu\mathrm{m}}$-[O IV]		$r_s = 0.674$
$L_{100\mu\mathrm{m}}$-[O IV]		$r_s = 0.586$
L_{FIR}-[O IV]		$r_s = 0.646$

Note. — r_s is the Spearman rank order correlation coefficient. The null probabilities are $P_r < 10^{-7}$ in all these correlations.

Table 4. Linear Regressions and Statistical Analysis for the [O IV], [Ne III] and [Ne II] Fluxes and Luminosities for the pure AGN Sources

	log [Ne III]		log [O IV]	
	a	b	a	b
Fluxes				
$\log F_{[Ne\ II]}$	0.81671	-2.5689	0.71895	-3.9149
	0.8 ± 0.1	2 ± 1	0.7 ± 0.1	-4 ± 2
	$r_s = 0.90$, $P_r = 4.4 \times 10^{-3}$		$r_s = 0.87$, $P_r = 5.8 \times 10^{-3}$	
Luminosities				
$\log L_{[Ne\ II]}$	0.86602	5.3088	0.82205	6.9797
	0.9 ± 0.1	5 ± 4	0.8 ± 0.1	7 ± 5
	$r_s = 0.945$, $P_r = 2.6 \times 10^{-3}$		$r_s = 0.945$, $P_r = 2.0 \times 10^{-3}$	
$\log L_{25\ \mu m}$			1.0395	0.97779
			1.0 ± 0.1	1 ± 6
$\log L_{60\ \mu m}$			0.79048	11.128
			0.8 ± 0.1	11 ± 6
$\log L_{100\ \mu m}$			0.66421	16.415
			0.7 ± 0.1	16 ± 6
$\log L_{FIR}$			0.74334	13.148
			0.7 ± 0.1	13 ± 6

Note. — The sources that shows no detectable PAH features at 6.2 μm and 11.5 μm in their spectra are: F15480-0344, IRAS00521-7054, MCG-2-8-39, MRK 3, MRK 9, NGC 3227, NGC 4941, NGC 526A, NGC 5548, NGC 7314 and UM 146. The regression coefficient (slope) and regression constant (intercept) are denoted by a and b, respectively. r_s is the Spearman rank order correlation coefficient and P_r is the null probability. For each relation we presented the exact linear regression values, the values as constrained by their statistical errors and the Spearman rank and null probability.